Aircraft System Identification from Multisine Inputs and Frequency Responses

Jared A. Grauer*
NASA Langley Research Center, Hampton, Virginia, 23681

Matthew J. Boucher†
NASA Armstrong Flight Research Center, Edwards, California, 93523

I. Introduction

The identification of aircraft flight dynamics is often performed using frequency responses, which are nonparametric models that quantify the steady-state magnitude and phase of a dynamic system response to sinusoidal inputs, as a function of frequency. Frequency responses are computed from measured input and output data, and then model parameters, such as stability and control derivatives, are estimated to best fit a parametric model to the empirical frequency response data. The utility of this approach is due to the familiarity of engineers with frequency responses, a number of theoretical and practical advantages under specific conditions, the availability of software packages, and many other reasons [1].

The standard procedure for identifying dynamic models of aircraft from frequency responses can be briefly summarized as the following: (1) apply frequency sweeps to single inputs, (2) estimate frequency responses using spectral techniques, and (3) identify model parameters by fitting a postulated model to Bode plots using a nonlinear optimization. Details and enhancements of this procedure can be found in Refs. [1–5].

A different excitation input, called orthogonal phase-optimized multisines [4], has become prevalent in aircraft flight testing because of the ability to excite multiple inputs simultaneously, which can reduce flight test time and costs. Multisine inputs were investigated for aircraft system identification using spectral estimation procedures in Refs. [6–9]. Rather than spectral estimation, Refs. [4, 10–12] proposed computing frequency responses using Fourier analysis and demonstrated real-time frequency response computation, stability margin monitoring, and fault detection. In Ref. [13], the Fourier analysis concept was extended for when aircraft are flown under closed-loop control or have mixers, which can correlate the inputs. In Ref. [14], maximum likelihood estimation was applied to frequency response data of open-loop aircraft to estimate coefficients in transfer functions and stability and control derivatives in state-space models. In Refs. [4, 10–14], one portion of the identification analysis using multisine inputs and frequency responses was extended.

In this work, the individual contributions in Refs. [4, 10–14] are unified as a different approach for aircraft system

*Research Engineer, Dynamic Systems and Control Branch, MS 308, Associate Fellow AIAA.
†Research Engineer, Controls and Dynamics Branch, MS 4840D, Member AIAA.

identification. The approach consists of (1) perturbing the inputs using multisines, (2) computing frequency responses using Fourier analysis, and (3) identifying model parameters and uncertainties using a maximum likelihood estimator. Advantages and drawbacks of the approach are discussed, as well as practical aspects learned during application to flight, wind tunnel, and simulation data.

This paper is organized as follows. Section II defines the problem statement. Section III briefly summarizes aircraft identification methods using frequency responses. Section IV presents details of the approach, which is demonstrated in Section V using a simulation example with multiple inputs and a feedback control law. Section VI summarizes the conclusions of the paper.

II. Problem Statement

Frequency responses are most commonly associated with linear time-invariant (LTI) systems. For aircraft flight dynamics, these types of models are valid for small perturbations about a reference flight condition and can be represented as the state-space model

$$\dot{\mathbf{x}}(t) = \mathbf{A}\,\mathbf{x}(t) + \mathbf{B}\,\mathbf{u}(t - \boldsymbol{\tau}_u) \tag{1a}$$

$$\mathbf{y}(t - \boldsymbol{\tau}_y) = \mathbf{C}\,\mathbf{x}(t) + \mathbf{D}\,\mathbf{u}(t - \boldsymbol{\tau}_u) \tag{1b}$$

where $\mathbf{u}(t)$ is a vector of n_u inputs, $\mathbf{x}(t)$ is a vector of n_x states, and $\mathbf{y}(t)$ is a vector of n_y outputs. The matrices $\mathbf{A}$, $\mathbf{B}$, $\mathbf{C}$, and $\mathbf{D}$ have constant elements and include the model parameters to be estimated. The vectors $\boldsymbol{\tau}_u$ and $\boldsymbol{\tau}_y$ contain time delays for the inputs and outputs, respectively.

The state-space model can alternatively be represented as a transfer function matrix by assuming zero initial conditions, applying the Laplace transform to Eq. (1), eliminating the state variable, and rearranging as

$$\mathbf{H}(s) = \frac{\mathbf{y}(s)}{\mathbf{u}(s)} = \left[\mathbf{C}\left(s\mathbb{I}_{n_x} - \mathbf{A}\right)^{-1}\mathbf{B} + \mathbf{D}\right] \circ \mathbf{T}(s) \tag{2}$$

In Eq. (2), $s = \sigma + j\omega$ is the Laplace variable, $\mathbb{I}_{n_x}$ is the $(n_x \times n_x)$ identity matrix, and $\circ$ denotes element-wise multiplication. The matrix $\mathbf{H}(s)$ is an $(n_y \times n_u)$ matrix of transfer functions $H_{ij}(s) = y_i(s)/u_j(s)$ and $\mathbf{T}(s)$ is an $(n_y \times n_u)$ matrix of transfer functions $T_{ij}(s) = e^{-\tau_{ij}s}$ where each time delay τ_{ij} is formed from the corresponding input and output time delays. Equation (2) is equivalent to Eq. (1) and is a complete description of the model.

Letting $\sigma = 0$ so that $s = j\omega$ simplifies the Laplace transform to the Fourier transform, which is a mapping of the dynamics onto steady sinusoids. This simplification discards information about the transient response of the system but

retains the steady-state response. Applying the Fourier transform to Eq. (2) yields the frequency response

$$\mathbf{H}(j\omega) = \frac{\mathbf{y}(j\omega)}{\mathbf{u}(j\omega)} = \left[\mathbf{C}\left(j\omega\mathbb{I}_{n_x} - \mathbf{A}\right)^{-1}\mathbf{B} + \mathbf{D}\right] \circ \mathbf{T}(j\omega) \tag{3}$$

Although the frequency response only characterizes the steady-state response of the system, it nonetheless contains all the information necessary to constitute the transfer function matrix in Eq. (2).

The complex-valued frequency response is often visualized as a Bode plot, where the magnitude and phase components

$$\|H_{ij}(j\omega)\| = 20\,\log_{10}\sqrt{\Re[H_{ij}(j\omega)]^2 + \Im[H_{ij}(j\omega)]^2} \tag{4a}$$

$$\angle H_{ij}(j\omega) = \frac{180}{\pi}\arctan\left(\frac{\Im[H_{ij}(j\omega)]}{\Re[H_{ij}(j\omega)]}\right) \tag{4b}$$

are shown as a function of frequency. In Eq. (4), $\Re$ and $\Im$ indicate real and imaginary parts of a complex number, and the Bode magnitude and phase components have units dB and deg, respectively.

The problem considered in this paper is to determine a parametric model of the aircraft based on frequency responses obtained from measurements, which involves computing $\mathbf{H}(j\omega)$ from $\mathbf{u}(t)$ and $\mathbf{y}(t)$, and then fitting a model to that data to estimate unknown parameters in $\mathbf{A}$, $\mathbf{B}$, $\mathbf{C}$, and $\mathbf{D}$.

III. Historical Perspectives

An early approach to system identification from frequency responses, called the frequency approach, involved dwell tests where a sinusoidal input was applied and steady-state responses developed after transients decayed [15]. The relative magnitude and phase at that frequency were computed by comparing input and output time histories. The first reported application to aircraft was Ref. [16], where the elevator was mechanically oscillated. This process was performed for several frequencies, inputs, and flight conditions to construct Bode plots in a simple and intuitive but time-consuming manner. Due to its reliability, this approach is still used in determining frequency responses of nonlinear simulation models.

Afterwards, Refs. [17–19] investigated the Fourier approach. Arbitrary inputs (e.g., pulses and doublets) were applied by the pilot, and then frequency responses were calculated as the ratio of Fourier transform data, as in Eq. (3). This approach was automated and used shorter durations of flight data than the frequency approach. However, several shortcomings were identified including errors from transient responses in the data, low input power at some frequencies, susceptibility to disturbances, and inaccuracies stemming from short time records [20, 21].

In the spectral estimation approach, spectral density functions are first estimated from input and output data, and then frequency responses and coherence functions are computed [1–5, 15, 22]. This approach has become standard practice

for identifying aircraft models from frequency responses and can be used with arbitrary inputs. Piloted frequency sweeps can produce good modeling data if the frequency is increased slowly and the system is well damped [21]. The analysis is typically formulated to produce unbiased estimates of the frequency response in the presence of uncorrelated measurement noise on the outputs [1], and requires the selection of various parameters, such as bin size or window size, shape, and overlap.

Once empirical frequency response data are obtained, a model structure can be postulated and unknown parameters in that model determined. In early works, straight-line approximations were used to fit models to Bode plots [23]. An iterative process using elementary transfer function factors was discussed in Ref. [24]. Reference [20] suggested using a nonlinear optimizer to match frequency responses. A similar strategy was applied in Ref. [25] to estimate parameters that fit data on a Bode plot, which was used for single-input single-output (SISO) systems and included tunable weights for trading accuracy between the Bode magnitude and phase fits. An enhanced version of this process using many transfer functions is detailed in Ref. [1]. The identification of model parameters by fitting complex-valued frequency response data was formalized for the maximum likelihood estimator in the frequency domain in Refs. [4, 26].

IV. Method

This section summarizes the system identification approach, including the multisine input design, frequency response calculations, and parameter estimation. The analysis used or was based on MATLAB software called System IDentification Programs for AirCraft [4, 27].

A. Input Design

The first step in the approach is to obtain informative flight test data. For identifying bare-airframe dynamics (control surface deflections to aircraft responses), excitation signals are applied to the command path at the actuators as shown in Fig. 1. The excitations used here are the orthogonal phase-optimized multisines developed in Refs. [28, 29] and discussed further in Refs. [4, 30].

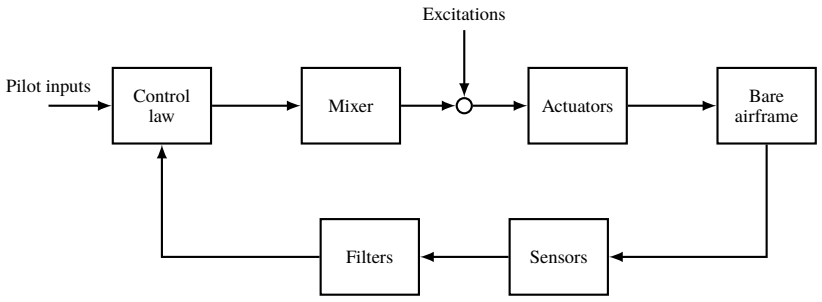

Fig. 1 Block diagram of the flight control architecture and excitation inputs.

Multisines are designed for a time duration T, which corresponds to a fundamental frequency $1/T$ and harmonic

frequencies k/T for integer values of k. A set K of n_f harmonic frequencies is selected over the bandwidth of interest. The frequency spacing is determined by T, where a longer record length increases the frequency resolution and decreases the lowest attainable frequency. Good modeling results usually need at least two cycles of each frequency, making $k = 2$ a practical lower limit, although higher values are preferable for increased rejection of random errors in the modeling. When there are multiple inputs to be excited simultaneously, K is divided into the subsets K_j with n_{f_j} frequencies.

Once the harmonics have been selected and assigned, each of the n_u multisine inputs is constructed as the sum of sinusoids

$$\mu_j(t) = \sum_{k \in K_j} a_k \sin\left(\frac{2\pi k}{T} t + \phi_k\right) \tag{5}$$

The amplitudes a_k define the power spectra of the multisines, and can be scaled to adjust the signal-to-noise ratios (SNRs) of the responses. The phase angles ϕ_k are individually optimized for minimum relative peak factor (RPF) to keep the aircraft near the reference flight condition, and then collectively shifted to start and end each input at zero.

Multisines are well suited for frequency response calculation. First, all inputs are excited at the same time, but in orthogonal ways, which can save time and cost relative to other inputs that are applied one at a time. Second, the optimization used to determine phase angles creates relatively small responses (for a given power spectrum), which is important for linear analysis. Third, multisines are similar to the classical dwell tests in that a steady-state response is developed. However, instead of using a single frequency on a single input, many frequencies are used on multiple inputs. Last, the input spectrum is concentrated at a set of discrete and known frequencies, which enables the relatively simple procedure for computing the frequency responses discussed next.

B. Frequency Response Computation

The second step in the identification is to compute frequency responses from measured data. This process starts by detrending measured time histories to reduce spectral leakage [2–4, 12]. Afterwards, the data are transformed into the frequency domain using the finite Fourier transform

$$z(j\omega) = \int_0^T z(t)\, e^{-j\omega t}\, dt \tag{6}$$

for each measured signal $z(t)$. In batch post-flight applications, Eq. (6) can be computed with high accuracy using a chirp z-transform with cubic interpolation of the measured data [4]. If the sampling frequency is much higher than the frequencies of interest, an Euler approximation of the integral

$$z(j\omega) \simeq \Delta t \sum_{i=1}^{N} z(t_i) e^{-j\omega t_i} \tag{7}$$

can also be used, where Δt is the sampling period and N is the number of samples. Fourier transforms are only evaluated for the n_f frequencies in K because only those frequencies have power in the steady-state response of an LTI system.

Rearranged, the first equality in Eq. (3) is

$$\mathbf{y}(j\omega) = \mathbf{H}(j\omega)\,\mathbf{u}(j\omega) \tag{8}$$

Evaluating Eq. (8) at the harmonic frequencies produces $n_y n_u n_f$ equations. When the aircraft is flown open loop and without mixing, many terms and equations are zero, due to the orthogonality of the inputs, leaving $n_y n_f$ non-zero equations to solve for the frequency response evaluations

$$H_{ij}(j\omega_k) = \left.\frac{y_i(j\omega_k)}{u_j(j\omega_k)}\right|_{K_j} \tag{9}$$

where $|_{K_j}$ denotes evaluation at frequencies associated with K_j. Equation (9) is the same as Eq. (3), except that the frequency response is only evaluated at the harmonic frequencies contained in the corresponding input. This formulation was used in Refs. [4, 10–12, 14].

Reference [31] demonstrated that when the aircraft is flown closed loop or with mixing, using Eq. (9) to compute the bare-airframe frequency responses produces inaccurate estimates. This is because the inputs for this case contain all the harmonic frequencies and Eq. (9) is deficient. Furthermore, no evaluations of Eq. (8) are zero, in general, and more information is needed to solve for the bare-airframe frequency responses.

This problem can be solved using the approach in Ref. [13], which was to assemble and append to Eq. (8) as

$$\begin{bmatrix} \mathbf{y}(j\omega)|_{K_1} \\ \mathbf{y}(j\omega)|_{K_2} \\ \vdots \\ \mathbf{y}(j\omega)|_{K_{n_u}} \\ \mathbf{0} \end{bmatrix} = \begin{bmatrix} \mathbf{U}_1 & \mathbf{0} & \dots & \mathbf{0} \\ \mathbf{0} & \mathbf{U}_2 & \dots & \mathbf{0} \\ \vdots & \vdots & \ddots & \vdots \\ \mathbf{0} & \mathbf{0} & \dots & \mathbf{U}_{n_u} \\ \mathbf{I}_1 & \mathbf{I}_2 & \dots & \mathbf{I}_{n_u} \end{bmatrix} \begin{bmatrix} \\ \mathrm{vec}[\mathbf{H}(j\omega)|_{K_1}] \\ \mathrm{vec}[\mathbf{H}(j\omega)|_{K_2}] \\ \vdots \\ \mathrm{vec}[\mathbf{H}(j\omega)|_{K_{n_u}}] \end{bmatrix} \tag{10}$$

where vec[.] indicates vectorization. In Eq. (10), each

$$\mathbf{U}_j = \begin{bmatrix} \mathbb{I}_{n_u} \otimes \mathrm{diag}[u_1(j\omega)|_{K_j}] & \mathbb{I}_{n_u} \otimes \mathrm{diag}[u_2(j\omega)|_{K_j}] & \dots & \mathbb{I}_{n_u} \otimes \mathrm{diag}[u_{n_u}(j\omega)|_{K_j}] \end{bmatrix} \tag{11}$$

where $\otimes$ is the Kronecker product operator and diag[.] constructs a diagonal matrix from a vector. The matrices $\mathbf{I}_j$ interpolate the frequency responses to harmonic frequencies not contained in the corresponding multisine input. For

appropriate multisine designs, linear interpolations are generally sufficient to achieve accurate frequency response estimates. The frequency response evaluations are then computed from Eq. (10) using matrix inversion. Equation (9) is recovered from Eq. (10) when the feedback gains are zero.

Computing frequency responses in this manner is related to the frequency approach and the Fourier approach, except that many frequencies are applied on multiple outputs, and the transforms are performed at the harmonic frequencies. This is a relatively simple analysis that can be performed in real time to produce the entire transfer function matrix from one maneuver [10–13].

Results degrade when nonlinearities (e.g., airspeed variation), time-varying dynamics (e.g., fuel burn), unmodeled inputs (e.g., atmospheric turbulence), measurement noise levels, or transient responses are present in the data at significant levels. The multisines should be adjusted or redesigned if SNRs were too low or if the frequency resolution was too coarse, respectively.

For the case without feedback, Eq. (9) is an unbiased estimate with variance inversely proportional to the SNR squared when there is no input measurement noise and when the output is in steady state for an integer number of cycles [32, 33]. The variance can be decreased further by running the input for additional cycles or increasing the multisine amplitudes if the responses remain within the linear region.

For the case with feedback or when input noise is significant, small biases result based on the input and output signal-to-noise ratios [33]. However, flight test results have shown good agreement between frequency responses and other methods for appropriately designed multisine excitations that create high SNRs at the harmonic frequencies [10, 13, 14].

Significant transient responses in the data can degrade frequency response results [10, 12]. Past experience flight testing flexible aircraft indicated it was best to wait for the aircraft to achieve steady-state oscillation, repeating the multisine excitation if necessary, and analyze integer numbers of cycles. Otherwise, the next best option was to ensure the time histories analyzed contained transient responses at both the onset and termination of the multisine excitations, which approximately canceled.

C. Maximum Likelihood Parameter Estimation

The third step is to estimate parameters in an LTI model that best fit the frequency response of the model to the empirical frequency response data. The approach taken here is based on the maximum likelihood method developed in Refs. [4, 26] and applied in Ref. [14] with multisine inputs.

The observation model is

$$\text{vec}\left[\mathbf{H}(j\omega_k)\right] = \text{vec}\left[\hat{\mathbf{H}}(j\omega_k)\right] + \mathbf{v}(j\omega_k) \tag{12}$$

where $\mathbf{H}(j\omega_k)$ are the empirical frequency responses and $\hat{\mathbf{H}}(j\omega_k)$ are the frequency responses of the model in Eq. (3)

for a set of parameters arranged in the vector $\boldsymbol{\theta}$. The modeling residual $\mathbf{v}(j\omega_k)$ are errors in the frequency responses and are assumed to be spectrally white, normally distributed, and stationary with

$$E\left[\mathbf{v}(j\omega_k)\right] = \mathbf{0} \tag{13a}$$

$$E\left[\mathbf{v}(j\omega_k)\,\mathbf{v}^{\dagger}(j\omega_k)\right] = \frac{1}{n_f}\,\mathbf{S}_{vv} \tag{13b}$$

where † denotes the complex-conjugate transpose. The matrix $\mathbf{S}_{vv}$ is the spectral density of $\mathbf{v}(t)$ and is fully populated because measurement noise on any particular input or output affects several frequency responses. Equation (13) is generally a good assumption if the flight test was conducted in low turbulence and the system remained within its linear region [13, 14].

The maximum likelihood estimator for this problem minimizes the cost

$$J(\boldsymbol{\theta}, \mathbf{S}_{vv}) = n_f \sum_{k\in K} \mathbf{v}^{\dagger}(j\omega_k)\,\mathbf{S}_{vv}^{-1}\,\mathbf{v}(j\omega_k) + n_f \ln|\mathbf{S}_{vv}| + n_y n_u n_f \ln\left(\frac{\pi}{n_f}\right) \tag{14}$$

Equation (14) is the negative log-likelihood function and is solved for $\boldsymbol{\theta}$ and $\mathbf{S}_{vv}$. Because the residuals minimized are errors in the frequency responses, this approach can be called the frequency response error (FRE) method, in analogy to other maximum likelihood estimators [4].

Optimization of Eq. (14) with respect to both $\boldsymbol{\theta}$ and $\mathbf{S}_{vv}$ at the same time typically exhibits convergence problems. Rather, a relaxation technique is used where the cost function is alternately optimized with respect to $\mathbf{S}_{vv}$ or $\boldsymbol{\theta}$, while holding the other constant, until results converge. For a given $\hat{\boldsymbol{\theta}}$, minimizing $J(\mathbf{S}_{vv})$ results in

$$\hat{\mathbf{S}}_{vv} = \left(\frac{\pi}{\omega_{n_f} - \omega_1}\right) \sum_{k\in K} \mathbf{v}(j\omega_k)\,\mathbf{v}^{\dagger}(j\omega_k) \tag{15}$$

Then for a given $\hat{\mathbf{S}}_{vv}$,

$$J(\boldsymbol{\theta}) = n_f \sum_{k\in K} \mathbf{v}^{\dagger}(j\omega_k)\,\hat{\mathbf{S}}_{vv}^{-1}\,\mathbf{v}(j\omega_k) \tag{16}$$

is minimized, which requires iteration using a nonlinear optimizer. For the Gauss-Newton method, the parameter update is

$$\hat{\boldsymbol{\theta}} = \hat{\boldsymbol{\theta}}_0 - \left[\mathbf{M}^{-1}\frac{\partial J}{\partial \boldsymbol{\theta}}\right]_{\boldsymbol{\theta}_0} \tag{17}$$

from the previous estimate $\hat{\boldsymbol{\theta}}_0$. Starting values for the model parameters may come from other analyses or prior information. In Eq. (17),

$$\mathbf{M} = 2n_f\,\Re\left[\sum_{k\in K} \mathbf{S}^{\dagger}(j\omega_k)\,\hat{\mathbf{S}}_{vv}^{-1}\,\mathbf{S}(j\omega_k)\right] \tag{18}$$

is the Fisher information matrix,

$$\frac{\partial J}{\partial \boldsymbol{\theta}} = -2n_f \, \Re \left[\sum_{k \in K} \mathbf{S}^{\dagger}(j\omega_k) \, \hat{\mathbf{S}}_{vv}^{-1} \, \mathbf{v}(j\omega_k) \right] \tag{19}$$

is the local cost gradient, and

$$\mathbf{S}(j\omega_k) = \frac{\partial}{\partial \boldsymbol{\theta}} \text{vec} \left[\hat{\mathbf{H}}(j\omega_k) \right] \tag{20}$$

is the frequency response sensitivity matrix obtained from analytical derivatives or numerical finite differences. The optimization is stopped when changes in the parameter estimates, cost function, cost gradient, and residual spectral density between iterations are sufficiently small.

The uncertainties in the parameter estimates are the Cramér-Rao bounds

$$\text{cov}(\hat{\boldsymbol{\theta}}) = \mathbf{M}^{-1} \tag{21}$$

where cov(.) is the covariance operator. The square-root of the diagonal terms are the parameter standard errors. Given an adequate model structure and accurate frequency response data, Eq. (21) is a realistic estimate of the parameter uncertainty levels and does not require corrections to match observed scatter in flight test data [14]. Furthermore, maximum likelihood estimators are asymptotically unbiased, consistent, efficient, and normal estimators [4]. Accuracy of the results can degrade if the errors do not have the characteristics assumed in Eq. (13), for example from significant model structure error.

Including prior information in the optimization is sometimes useful for combining results from other analyses or multiple maneuvers, or when there is not enough information present in the data to accurately estimate all of the unknown parameters. In this case, Eqs. (16)–(18) are modified to account for the prior estimate and uncertainty, $\boldsymbol{\theta}_p$ and $\boldsymbol{\Sigma}_p$, as [4, 26]

$$J(\boldsymbol{\theta}) = n_f \sum_{k \in K} \mathbf{v}^{\dagger}(j\omega_k) \, \hat{\mathbf{S}}_{vv}^{-1} \, \mathbf{v}(j\omega_k) + n_f \left(\boldsymbol{\theta} - \boldsymbol{\theta}_p \right)^T \boldsymbol{\Sigma}_p^{-1} \left(\boldsymbol{\theta} - \boldsymbol{\theta}_p \right) \tag{22a}$$

$$\hat{\boldsymbol{\theta}} = \hat{\boldsymbol{\theta}}_0 - \left(\mathbf{M} + \boldsymbol{\Sigma}_p^{-1} \right)^{-1} \left[\frac{\partial J}{\partial \boldsymbol{\theta}} + \boldsymbol{\Sigma}_p^{-1} \left(\boldsymbol{\theta} - \boldsymbol{\theta}_p \right) \right] \tag{22b}$$

$$\mathbf{M} = 2n_f \, \Re \left[\sum_{k \in K} \mathbf{S}^{\dagger}(j\omega_k) \, \hat{\mathbf{S}}_{vv}^{-1} \, \mathbf{S}(j\omega_k) \right] + \boldsymbol{\Sigma}_p^{-1} \tag{22c}$$

Multiple maneuvers may also be processed simultaneously to estimate a single set of model parameters for the entire data set. This is done by computing frequency response data for each maneuver, and then stacking them in Eq. (12) as additional frequency responses to be matched. In this case, $\mathbf{S}_{vv}$ has $(n_y n_u \times n_y n_u)$ block matrices along its diagonal and is zero elsewhere. The multisine inputs do not need to contain the same harmonic frequencies for each maneuver. If the model parameters are nondimensional stability and control derivatives, an accurate estimation can be performed for

maneuvers conducted at different flight conditions.

D. Further Discussion

The approach described has advantages and drawbacks relative to other approaches for aircraft system identification. Many of these aspects are discussed in Refs. [1, 4, 12, 26, 33].

An important advantage of computing frequency responses is insight into the model structure of the dynamics over the bandwidth of interest. This can be helpful for determining the order of the model and rough estimates for starting parameters. Other dynamics, disturbances, and noise outside the bandwidth of interest are automatically removed from the modeling data during the frequency transformation.

Computing frequency responses and using the FRE estimator may be performed as a preliminary analysis, before moving on to an output-error analysis. Only the harmonic frequencies are analyzed in FRE, leading to iterations that run quickly. Furthermore, the equations of motion do not have to be solved, which can take long amounts of time for systems with many frequencies to analyze and outputs to match, such as aeroelastic aircraft [34, 35].

The main disadvantage of this method is that it can only be applied using LTI models. Furthermore, a long periods of flight test time could be required if there are many inputs and very lightly damped resonances in the bare-airframe dynamics. The matching of frequency responses, rather than directly measured time series or their Fourier transforms, requires additional processing that can introduce errors. Lastly, application of this approach requires computerized multisines added at the actuators, a capability that is prevalent on modern research aircraft.

V. Numerical Example

The approach is demonstrated using a simulation example. The NASA T-2 airplane, shown in Fig. 2 and described in Table 1, is a dynamically-scaled 5.5% version of a generic commercial transport aircraft that has been used extensively for flight research [30].

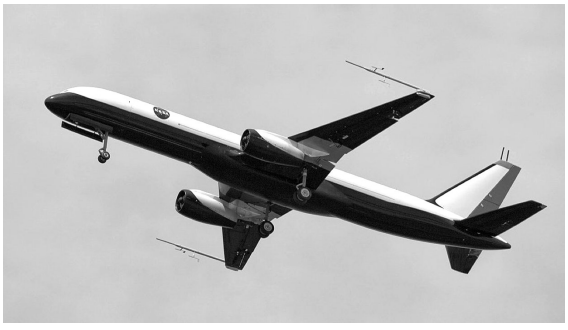

Fig. 2 T-2 airplane (credit: NASA Langley Research Center).

Table 1 T-2 geometry and nominal mass properties.

Symbol	Value	Unit
b	6.849	ft
$\bar{c}$	0.915	ft
S	5.902	ft^2
m	1.585	slug
I_{xx}	1.179	slug-ft^2
I_{yy}	4.520	slug-ft^2
I_{zz}	5.527	slug-ft^2
I_{xz}	0.211	slug-ft^2

An LTI state-space model of the bare-airframe short period dynamics is [4]

$$\begin{bmatrix} \dot{\alpha} \\ \dot{q} \end{bmatrix} = \begin{bmatrix} \frac{\bar{q}S}{mV} C_{Z_\alpha} & 1 + \frac{\bar{q}S}{mV}\frac{\bar{c}}{2V} C_{Z_q} \\ \frac{\bar{q}S\bar{c}}{I_{yy}} C_{m_\alpha} & \frac{\bar{q}S\bar{c}}{I_{yy}}\frac{\bar{c}}{2V} C_{m_q} \end{bmatrix} \begin{bmatrix} \Delta\alpha \\ q \end{bmatrix} + \begin{bmatrix} \frac{\bar{q}S}{mV} C_{Z_{\delta_{eo}}} & \frac{\bar{q}S}{mV} C_{Z_{\delta_{ei}}} \\ \frac{\bar{q}S\bar{c}}{I_{yy}} C_{m_{\delta_{eo}}} & \frac{\bar{q}S\bar{c}}{I_{yy}} C_{m_{\delta_{ei}}} \end{bmatrix} \begin{bmatrix} \Delta\delta_{eo} \\ \Delta\delta_{ei} \end{bmatrix} \tag{23a}$$

$$\begin{bmatrix} q \\ \Delta a_z \end{bmatrix} = \begin{bmatrix} 0 & 1 \\ \frac{\bar{q}S}{mg} C_{Z_\alpha} & \frac{\bar{q}S}{mg}\frac{\bar{c}}{2V} C_{Z_q} \end{bmatrix} \begin{bmatrix} \Delta\alpha \\ q \end{bmatrix} + \begin{bmatrix} 0 & 0 \\ \frac{\bar{q}S}{mg} C_{Z_{\delta_{eo}}} & \frac{\bar{q}S}{mg} C_{Z_{\delta_{ei}}} \end{bmatrix} \begin{bmatrix} \Delta\delta_{eo} \\ \Delta\delta_{ei} \end{bmatrix} \tag{23b}$$

The states are angle of attack α and pitch rate q. The inputs δ_{eo} and δ_{ei} are the outboard and inboard elevators, respectively, which are formed by moving four left and right control surfaces on the trailing edge of the horizontal tail as symmetric pairs. The outputs are q and vertical acceleration at the center of mass, a_z. Angle of attack and pitch angle measurements were not included to keep this example problem smaller in size. Perturbations from the flight condition are represented with Δ. The terms inside the matrices are constants for a given flight condition, where the nondimensional stability and control derivatives were estimated from flight test data at 1270 ft altitude, 130 ft/s airspeed, and 4.0 deg angle of attack.

Actuator models were included as first-order lags with poles at 5 Hz and time delays of 0.01 s. Measurement noise with standard deviations listed in Table 2 were added to the measurements. The q measurement was fed back to δ_{ei} with a gain of -0.2 to change the short-period damping ratio and frequency from 0.43 and 5.9 rad/s (0.94 Hz) to 0.70 and 8.0 rad/s (1.3 Hz), respectively.

Table 3 lists parameters for outboard and inboard multisine inputs. The excitations were designed for about a 2 deg input amplitude and a 10 s duration, giving a 0.1 Hz frequency resolution. The excitation bandwidth was selected as between 0.4 and 2.1 Hz, which encloses the short period natural frequency and provides adequate cycles for noise rejection and decay of transient responses. This design had 9 excitation frequencies per input, resulting in 36 data points for the FRE estimation.

Table 2 Measurement noise levels.

Measurement	Standard deviation	Unit
δ_{eo}, δ_{ei}	0.026	deg
α	0.051	deg
q	0.20	deg/s
θ	0.010	deg
a_z	0.0026	g

Table 3 Multisine design parameters (T = 10 s).

Outboard elevator RPF = 1.04			Inboard elevator RPF = 1.11		
a_k, deg	k	ϕ_k, rad	a_k, deg	k	ϕ_k, rad
0.11	4	2.79	0.11	5	0.96
0.11	6	5.67	0.11	7	3.16
0.11	8	5.00	0.11	9	0.24
0.11	10	0.97	0.11	11	2.72
0.11	12	0.59	0.11	13	3.21
0.11	14	0.39	0.11	15	0.02
0.11	16	5.01	0.11	17	5.80
0.11	18	0.12	0.11	19	0.04
0.11	20	2.87	0.11	21	4.89

Simulated measurements, sampled at 50 Hz, are shown in Fig. 3. For reference, time histories of α and the Euler pitch angle θ are also shown. The excitation was started after 2 s. The control surface deflections and aircraft responses were small perturbations from the steady values for this flight condition.

Figure 4 shows frequency responses between the measured inputs and outputs. The solid black lines are the true frequency responses obtained from the bare-airframe model in Eq. (23) using the true values of the model parameters. The open blue circles are the frequency response estimates obtained from the measurements using Eq. (9), which does not account for the feedback, whereas the solid blue circles used Eq. (10), which does account for the feedback. Estimates using Eq. (9) are incorrect for frequency responses from δ_{eo} due to input correlation from the feedback. The estimates from δ_{ei} and all the estimates computed using Eq. (10) were in close agreement with the true frequency responses, with coefficients of determination above $R^2 = 0.99$ and differences in Bode plot magnitudes and phase angles less than 0.3 dB and 2.0 deg.

The FRE method was used to determine nondimensional stability and control derivatives in Eq. (23) that best matched the model frequency response to the data obtained using Eq. (10). The estimator was initialized using parameter estimates obtained from an equation-error analysis. Results converged in 19 iterations, which used about 0.8 s on a

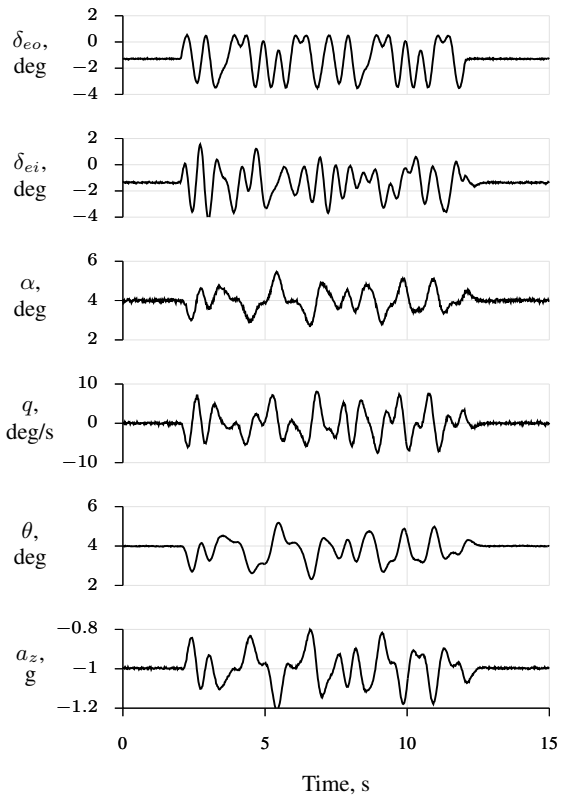

Fig. 3 Simulated measurement time histories.

standard laptop. The fitted model is shown in Fig. 4 as red dashed lines. These fits had greater than $R^2 = 0.99$ and differences in Bode plot magnitudes and phase angles less than 0.1 dB and 0.7 deg. Due to the additional information inherent in the parametric model structure, the identified model matched the true frequency responses more accurately than the non-parametric frequency response data used in the modeling.

A comparison of parameter estimates is given in Table 4. The first two columns list the nondimensional stability derivatives and their true values used in the simulation. The third column shows the estimates obtained using FRE, which were all within two standard errors of the true values. The standard errors were under 1% except for C_{Z_q} (42%), $C_{Z_{\delta_{eo}}}$ (12%), and $C_{Z_{\delta_{ei}}}$ (6.4%), which are typically difficult to accurately estimate and are often removed from the model structure.

For further comparison, four additional sets of estimates are also given in Table 4 using these data. The first set used output error in the time domain (TOE) to match 1502 samples of output data and converged in 14 iterations and 0.5 s. The second set used output error in the frequency domain (FOE) to match 170 samples of output Fourier transform data between 0.2 to 2.3 Hz, in 0.025 Hz increments, and converged in 14 iterations and 0.2 s. The third set also applied FOE, but only used the same 36 frequencies used by FRE and converged in 12 iterations and 0.1 s. The fourth set, BPE, matched Bode magnitude and phase plots at the harmonic frequencies, where the phase angles were weighted by 0.02 relative to the magnitudes [36], and converged in 5 iterations and 0.2 s.

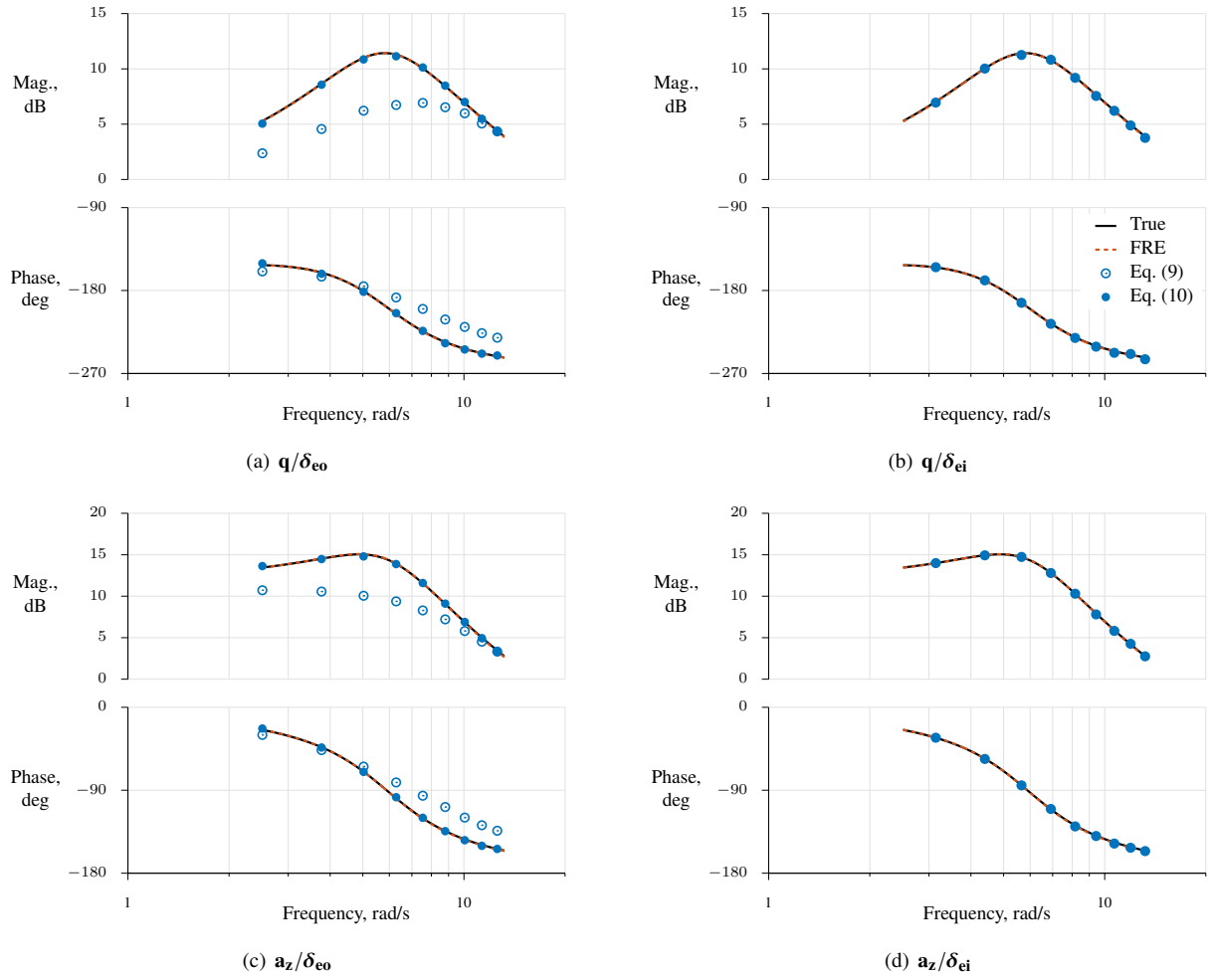

(a) $\mathbf{q}/\boldsymbol{\delta}_{\mathbf{eo}}$ (b) $\mathbf{q}/\boldsymbol{\delta}_{\mathbf{ei}}$

(c) $\mathbf{a_z}/\boldsymbol{\delta}_{\mathbf{eo}}$ (d) $\mathbf{a_z}/\boldsymbol{\delta}_{\mathbf{ei}}$

Fig. 4 Frequency response estimates and fits using FRE.

Table 4 Parameter estimates and standard errors.

Parameter	True value	FRE	TOE	FOE*	FOE†	BPE†
C_{Z_α}	−3.89	−3.92 ± 0.039	−3.92 ± 0.039	−3.90 ± 0.060	−3.91 ± 0.054	−3.82 ± 0.048
C_{Z_q}	−5.17	−3.86 ± 1.6	−4.64 ± 0.46	−4.49 ± 2.2	−4.01 ± 1.9	−2.02 ± 1.1
$C_{Z_{\delta_{eo}}}$	−0.170	−0.173 ± 0.021	−0.168 ± 0.0040	−0.167 ± 0.018	−0.162 ± 0.014	−0.104 ± 0.027
$C_{Z_{\delta_{ei}}}$	−0.170	−0.173 ± 0.012	−0.168 ± 0.0036	−0.165 ± 0.017	−0.167 ± 0.014	−0.111 ± 0.027
C_{m_α}	−1.30	−1.29 ± 0.0054	−1.29 ± 0.0027	−1.29 ± 0.0089	−1.29 ± 0.0079	−1.28 ± 0.0026
C_{m_q}	−37.1	−37.6 ± 0.39	−37.0 ± 0.21	−36.9 ± 0.74	−36.9 ± 0.63	−38.2 ± 0.34
$C_{m_{\delta_{eo}}}$	−0.806	−0.799 ± 0.0060	−0.800 ± 0.0027	−0.798 ± 0.0098	−0.798 ± 0.0088	−0.824 ± 0.025
$C_{m_{\delta_{ei}}}$	−0.806	−0.801 ± 0.0064	−0.800 ± 0.0027	−0.798 ± 0.0097	−0.797 ± 0.0087	−0.828 ± 0.025

*Using frequencies 0.2, 0.225, . . . , 2.3 Hz.
†Using only the harmonic frequencies.

Except for the TOE estimate of C_{m_α} and most of the BPE estimates, the estimates were within two standard errors of the true values. The TOE estimates also had smaller uncertainty levels because significantly more data points were available for analysis. In application to experimental data, additional processing is performed to account for colored residuals in the uncertainty calculations in the time-domain output-error analysis [4].

Because output error methods can use transient response data, unlike methods based on frequency responses, FOE benefits from additional samples of the Fourier transforms. Results were similar between the two sets of FOE estimates, but using the higher-resolution frequency sampling improved the average parameter estimate by 1.4%. However, due to using additional samples of the Fourier transform at lower signal-to-noise ratios, the average parameter standard errors also increased by 0.89%. The FRE results were similar to both of the FOE results, and had 0.05% more average parameter error and 0.78% less average parameter standard error than the low-resolution FOE estimates.

The frequency response methods used more time per iteration than the output error methods here because the estimation problem was relatively small, and because FRE and BPE matched four outputs (frequency responses from two inputs to two outputs), whereas TOE and FOE matched only two outputs (measured responses). This reduced the number of sensitivity equations calculated from finite differences. Larger estimation problems with many inputs, outputs, and harmonic frequencies have resulted in FRE converging in less time than FOE [34, 35].

Selecting the weights for the BPE estimates, rather than computing them from the model residuals, resulted in faster convergence of the estimation results. However, these estimates had larger bias than the other methods and the uncertainty bounds were not reliable because the cost function was not a maximum likelihood estimator. The nonlinear transformations used in Eq. (4) to compute Bode plots from frequency responses introduced a nonlinear weighting of the errors in the estimation, for which a coherence weighting could be applied when the frequency responses are computed using spectral estimation [1].

VI. Conclusions

An approach for identifying dynamic models of aircraft from measured data was presented. The aircraft dynamics are excited using orthogonal phase-optimized multisines, frequency responses are computed as ratios of output to input Fourier transform data at the multisine harmonic frequencies, and a maximum likelihood estimator is used to determine parameters and associated uncertainties that best match the frequency responses. The approach was demonstrated using a simulation example, and applications to flight test data were referenced.

The approach is limited to the identification of linear time-invariant systems, flight in low levels of turbulence, and aircraft with the capability to inject computerized inputs to the command path at the actuators.

The main benefit of the approach is that empirical frequency responses are simultaneously obtained from multiple inputs during one maneuver, which can be conducted either in open loop or under closed-loop control. This capability can shorten flight test durations and save time and costs. Furthermore, the frequency response data are relatively simple

to compute and yield information on the model structure, which can be used in the frequency response-error estimator described in this work or other parameter estimation analyses.

Acknowledgments

This research was supported by the NASA Advanced Air Transport Technology (AATT) project. Eugene Morelli and Rose Weinstein provided helpful reviews of this paper.

References

[1] Tischler, M., and Remple, R., *Aircraft and Rotorcraft System Identification: Engineering Methods with Flight Test Examples*, 2nd ed., AIAA, Reston, VA, 2012. doi:10.2514/4.868207.

[2] Bendat, J., and Piersol, A., *Random Data: Analysis and Measurement Procedures*, 2nd ed., John Wiley & Sons, New York, NY, 1986, pp. 164–324.

[3] Press, W., Teukolsky, S., Vetterling, W., and Flannery, B., *Numerical Recipes*, Cambridge University Press, New York, NY, 1986, pp. 381–453.

[4] Morelli, E., and Klein, V., *Aircraft System Identification: Theory and Practice*, 2nd ed., Sunflyte, Williamsburg, VA, 2016.

[5] Klyde, D., and Schulze, P., "Determining Handling Qualities Parameters: Lessons from the Frequency Domain," AIAA Paper 2020-0508, 2020. doi:10.2514/6.2020-0508.

[6] Young, P., and Patton, R., "Comparison of Test Signals for Aircraft Frequency Domain Identification," *Journal of Guidance, Control, and Dynamics*, Vol. 13, No. 3, 1990, pp. 430–438. doi:10.2514/3.25355.

[7] Heeg, J., and Morelli, E., "Evaluation of Simultaneous Multisine Excitation of the Joined Wing SensorCraft Aeroelastic Wind Tunnel Model," AIAA Paper 2011-1959, 2011. doi:10.2514/6.2011-1959.

[8] Ivler, C., Rowe, E., Martin, J., Lopez, M., and Tischler, M., "System Identification Guidance for Multirotor Aircraft: Dynamic Scaling and Test Techniques," VFS Paper 239, 2019.

[9] Lichota, P., Szulcyk, J., Tischler, M., and Berger, T., "Frequency Response Identification from Multi-Axis Maneuver with Simultaneous Multisine Inputs," *Journal of Guidance, Control, and Dynamics*, Vol. 42, No. 11, 2019, pp. 2550–2556. doi:10.2514/1.G004346.

[10] Grauer, J., and Morelli, E., "Method for Real-Time Frequency Response and Uncertainty Estimation," *Journal of Guidance, Control, and Dynamics*, Vol. 37, No. 1, 2014, pp. 336–343. doi:10.2514/1.60795.

[11] Grauer, J., "Aircraft Fault Detection using Real-Time Frequency Response Estimation," AIAA Paper 2016-0372, 2016. doi:10.2514/6.2016-0372.

[12] Morelli, E., and Grauer, J., "Practical Aspects of Frequency-Domain Approaches for Aircraft System Identification," *Journal of Aircraft*, Vol. 57, No. 2, 2020, pp. 268–291. doi:10.2514/1.C035599.

[13] Grauer, J., and Boucher, M., "Real-Time Estimation of Bare-Airframe Frequency Responses from Closed-Loop Data and Multisine Inputs," *Journal of Guidance, Control, and Dynamics*, Vol. 43, No. 2, 2019, pp. 288–298. doi:10.2514/1.G004574.

[14] Grauer, J., "Dynamic Modeling using Output-Error Parameter Estimation based on Frequency Responses Estimated with Multisine Inputs," NASA TM-2018-220108, November 2018.

[15] James, H., Nichols, N., and Phillips, R., *Theory of Servomechanisms*, McGraw-Hill, New York, NY, 1947, pp. 262–307.

[16] Milliken, W., "Progress in Dynamic Stability and Control Research," *Journal of the Aeronautical Sciences*, Vol. 14, No. 9, 1947, pp. 493–519. doi:10.2514/8.1434.

[17] Seamans, R., Bromberg, B., and Payne, L., "Application of the Performance Operator to Aircraft Automatic Control," *Journal of the Aeronautical Sciences*, Vol. 15, No. 9, 1948, pp. 535–555. doi:10.2514/8.11644.

[18] Seamans, R., Blasingame, B., and Clementson, G., "The Pulse Method for the Determination of Aircraft Dynamic Performance," *Journal of the Aeronautical Sciences*, Vol. 17, No. 1, 1950, pp. 22–38. doi:10.2514/8.1514.

[19] LaVerne, M., and Boksenbom, A., "Frequency Response of Linear Systems from Transient Data," NACA TR-977, September 1950.

[20] Greenberg, H., "A Survey of Methods for Determining Stability Parameters of an Airplane from Dynamic Flight Measurements," NACA TN 2340, April 1951.

[21] Eggleston, J., and Mathews, C., "Application of Several Methods for Determining Transfer Functions and Frequency Response of Aircraft from Flight Data," NACA TR 1204, January 1954.

[22] Tukey, J., "The Sampling Theory of Power Spectrum Estimates," No. NAVEXOS-P-735 in Symposium on Applications of Autocorrelation Analysis to Physical Problems, Office of Naval Research, Woods Hole, MA, 1949.

[23] Lees, S., "Graphical Aids for the Graphical Representation of Functions of the Imaginary Argument," MIT Engineering Memorandum E-25, February 1951.

[24] Bruns, R., and Saunders, R., *Analysis of Feedback Control Systems: Servomechanisms and Automatic Regulators*, McGraw-Hill, New York, NY, 1955, pp. 269–313.

[25] Hodgkinson, J., LaManna, W., and Heyde, J., "Handling Qualities of Aircraft with Stability and Control Augmentation Systems — A Fundamental Approach," *Aeronautical Journal*, Vol. 80, No. 782, 1976, pp. 75–81. doi:10.1017/S0001924000033510.

[26] Klein, V., "Aircraft Parameter Estimation in Frequency Domain," AIAA Paper 78-1344, 1978. doi:10.2514/6.1978-1344.

[27] Morelli, E., "System IDentification Programs for AirCraft (SIDPAC)," version 4.1, NASA Software Catalog, `http://software.nasa.gov`, accessed Jun. 2020.

[28] Morelli, E., "Multiple Input Design for Real-Time Parameter Estimation in the Frequency Domain," IFAC Paper REG-360, 2003. doi:10.1016/S1474-6670(17)34833-4.

[29] Morelli, E., "Flight-Test Experiment Design for Characterizing Stability and Control of Hypersonic Vehicles," *Journal of Guidance, Control, and Dynamics*, Vol. 32, No. 3, 2009, pp. 949–959. doi:10.2514/1.37092.

[30] Morelli, E., "Flight Test Maneuvers for Efficient Aerodynamic Modeling," *Journal of Aircraft*, Vol. 49, No. 6, 2012, pp. 1857–1867. doi:10.2514/1.C031699.

[31] Berger, T., Tischler, M., Knapp, M., and Lopez, M., "Identification of Multi-Input Systems in the Presence of Highly Correlated Inputs," *Journal of Guidance, Control, and Dynamics*, Vol. 41, No. 10, 2018, pp. 2247–2257. doi:10.2514/1.G003530.

[32] Ljung, L., *System Identification: Theory for the User*, 2nd ed., Prentice Hall, Upper Saddle River, NJ, 1999, pp. 168–196. doi:10.1109/MRA.2012.2192817.

[33] Pintelon, R., and Schoukens, J., *System Identification: A Frequency Domain Approach*, 2nd ed., John Wiley & Sons, Hoboken, NJ, 2012, pp. 33–72. doi:10.1002/9781118287422.

[34] Grauer, J., and Boucher, M., "Identification of Aeroelastic Models for the X-56A Longitudinal Dynamics Using Multisine Inputs and Output Error in the Frequency Domain," *Aerospace*, Vol. 6, No. 24, 2019, pp. 1–25. doi:10.3390/aerospace6020024.

[35] Grauer, J., and Boucher, M., "System Identification of Flexible Aircraft: Lessons Learned from the X-56A Phase 1 Flight Tests," AIAA Paper 2020-1017, 2020. doi:10.2514/6.2020-1017.

[36] Anon., "Military Standard — Flying Qualities of Piloted Aircraft," Tech. Rep. MIL-STD-1797A, Department of Defense, January 1990.